# DENSITY RATIO AND VELOCITY RATIO EFFECTS ON THE STRUCTURE OF TRANSVERSE JETS IN SUPERSONIC CROSSFLOW

**Mirko Gamba**
Department of Aerospace Engineering,
University of Michigan
Ann Arbor, MI, USA
mirkog@umich.edu

**Victor A. Miller**
Mechanical Engineering Department,
Stanford University
Stanford, CA, USA
vamiller@stanford.edu

**M. Godfrey Mungal**
School of Engineering,
Santa Clara University
Santa Clara, CA, USA
Mechanical Engineering Department,
Stanford University
Stanford, CA, USA
mungal@stanford.edu

## ABSTRACT

It is generally accepted that the jet-to-crossflow momentum flux ratio, $J$, is the primary parameter describing the structure, penetration and mixing properties of transverse jets. The interplay between density and velocity ratios, at a given $J$, on these properties is, however, seldom considered nor fully understood. The current experimental work explores this interplay on transverse underexpanded sonic jets in a supersonic nitrogen crossflow ($M = 2.3$, $T = 460\ K$). A single-excitation, dual-band detection PLIF imaging scheme of toluene seeded into the crossflow is used to mark the crossflow fluid mixing into the transverse jet fluid and to determine the local fluid temperature. Different values of density and velocity ratios, while maintaining a constant value of $J$ (equal to 2.4), are investigated by injecting gases with different molecular weights. Notwithstanding the fact that all cases have the same value of $J$ and some similarity on the penetration characteristics exists, the emerging picture of the instantaneous turbulent structure of the flow indicates that the dynamics of entrainment and local mixing might be altered by low (high) values of the density (velocity) ratio compared to the corresponding case at high (low) values.

## INTRODUCTION

A transverse jet in crossflow is one of the canonical flows in fluid dynamics and covers an important role in many engineering applications. The jet in crossflow, or simply JICF, system arises when fluid is injected into a crossflow. Injection can be perpendicular or angled relative to the incoming crossflow. In the supersonic case, what we refer to here as the jet in supersonic crossflow, or JISCF, and what we consider in this study, both injection and crossflow might be supersonic. Recent reviews on the general properties of JICF, and to some extent on what is known on the JISCF, give an up-to-date summary of their current understanding (Karagozian, 2010; Mahesh, 2013).

It is well-known that the flowfield of a JICF is controlled by a complex system of large-scale vortical structures (see for example Fric & Roshko, 1994). In turn, these structures dictate the dynamics and properties of the overall system, including the underlying entrainment, turbulent transport and mixing (Smith & Mungal, 1998; Su & Mungal, 2004). Similar considerations extend to the supersonic case (Gruber *et al.*, 1996; Ben-Yakar *et al.*, 2006).

In the supersonic case, the underlying vortical features of the JISCF remain mostly unchanged, but now a complex system of shock waves exists from the interaction (blockage) of the jet with the supersonic crossflow, the boundary layer, and the expansion of the jet (for sonic and/or underexpanded injection). A schematic diagram of the large-scale structure of a JISCF is shown in Fig. 1. As a result of the shock system and its dynamics, the flow structure, topology, and properties of the transverse jet are affected.

Momentum conservation arguments (for example, Broadwell & Breidenthal, 1984; Hasselbrink & Mungal, 2001) predict that the properties of a JICF are captured by jet-to-crossflow momentum flux ($J$) scaling laws. Similar models have also been constructed for the supersonic case (e.g., Schetz & Billig, 1966). This parameter groups two quantities, the jet-to-crossflow velocity ratio ($r$) and density ratio ($s$): $J = sr^2$.

In particular, global properties such as the (mean) jet penetration trajectory, velocity and concentration decays are expected to scale with $J$ alone. Experimental observation typically support this reasoning, even in the supersonic case (Portz & Segal, 2006; Mahesh, 2013). Because these models are based on momentum conservation under the assumption of entrainment and mixing processes between jet and

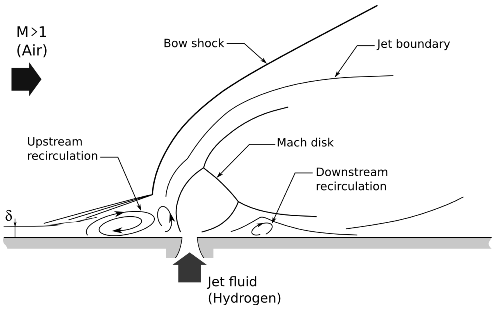


Figure 1: Schematic diagram of the flowfield of a transverse jet in supersonic crossflow.

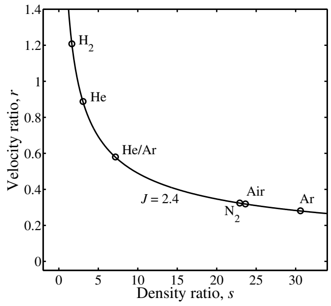


Figure 2: Velocity ratio – density ratio curve at constant $J$= 2.4.

crossflow fluids, they also imply that the underlying entrainment and small-scale mixing are somewhat independent of the specific details of the transverse jet (for example $r$ or $s$) but they only depend on $J$.

Therefore, under this classical view, two JISCFs with the same values of $J$, but different values of ($s$, $r$), should be identical. In particular, they should have the same transverse penetration, which then implies they undergo the same mixing process. This would be the case where two jets are generated by injection of dissimilar fluids at the same $J$; for example, injecting a light or heavy fluid into the supersonic crossflow such that the values of $s$ (and hence $r$) are different (i.e., low or large molecular weight, for example hydrogen and argon). However, the limited work available seems to suggest something different, and the current work aims at further exploring this issue.

Some recent work on the incompressible transverse jet is now shedding some light on the separate effect of $s$ and $r$ on the stability and mixing properties of low speed, low Reynolds number JICF in same- and different-density configurations that cannot be captured by a description solely based on $J$ (Megerian *et al.*, 2007; Getsinger *et al.*, 2012). For the supersonic case, previous studies considering injection of dissimilar fluids (at constant $J$) have found that the time-average global properties are nearly the same and consistent with a $J$ scaling (Gruber *et al.*, 1996). Examples are the penetration and average concentration distribution that are found to be weakly dependent on the injectant (Gruber *et al.*, 1997; Watanabe *et al.*, 2012). On the other hand, there is also some evidence that the instantaneous structure and coherence of the scalar field may in fact depend on injectant (for example, helium versus air) (Gruber *et al.*, 1997; Ben-Yakar *et al.*, 2006). Furthermore, the characteristics of the velocity field, turbulent fluctuations and intermittent properties also appear to depend on the injectant type (Watanabe *et al.*, 2012).

The work presented here is an experimental effort aimed at exploring the interplay of $J$, $s$, and $r$ on the characteristics, mixing, and structure of transverse underexpanded sonic jets in a supersonic crossflow (at $M_{cf}$ = 2.3). A single-excitation, dual-band detection PLIF imaging scheme of toluene seeded into the crossflow is used to mark the crossflow fluid mixing into the transverse jet fluid and to determine the local fluid temperature. Different values of density ratio and velocity ratio, while maintaining a constant value of $J$ (equal to 2.4), are investigated. The different ($s$, $r$) combinations are generated by injecting gases with different molecular weights into the same crossflow. The investigated parameter space ($s$, $r$) at constant $J$ is summarized in Fig. 2 where a constant $J$= 2.4 curve is shown. In the next section, a brief description of the experimental set up is presented. Following this, results and discussion are presented.

## EXPERIMENTAL SETUP

In this section we will give a brief description of the experimental configuration, the JISCF system, the flow facility, and we will describe the toluene PLIF technique as applied for this investigation.

### Transverse jet in supersonic crossflow

The experiments presented herein were conducted at the 6” Expansion Tube Facility of the High Temperature Gasdynamics Laboratory at Stanford University. A description of this flow facility can be found in Heltsley *et al.* (2006). With reference to Fig. 1, the flow of interest was generated by issuing a jet of fluid perpendicularly from a flat plate into a supersonic crossflow produced by the expansion tube. Injection was carried out from room temperature (i.e., the stagnation temperature of the jet was near 295 $K$) conditions at a suitable value of the jet stagnation pressure (around 1.9 $MPa$, depending upon the fluid being used). The flat plate (155 $mm$ long by 100 $mm$ wide) was placed at the exit of the expansion tube within the region of uniform flow. The jet fluid was injected from a contoured round orifice 2 $mm$ in diameter ($D$) located 64 $mm$ from the leading edge of the flat plate. Different values of $s$ and $r$ were investigated by injecting gases with different molecular weights while maintaining a constant value of $J$=2.4. To explore a range of ($s$,$r$) cases, injection of hydrogen, helium, (85%/15%) helium/argon mixture, nitrogen, air and argon were considered; these cases correspond to a range

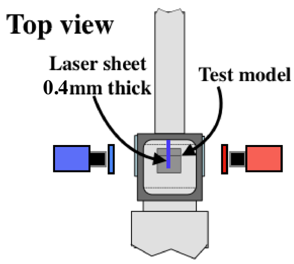


Figure 3: Schematic diagram of the experimental and imaging configuration.

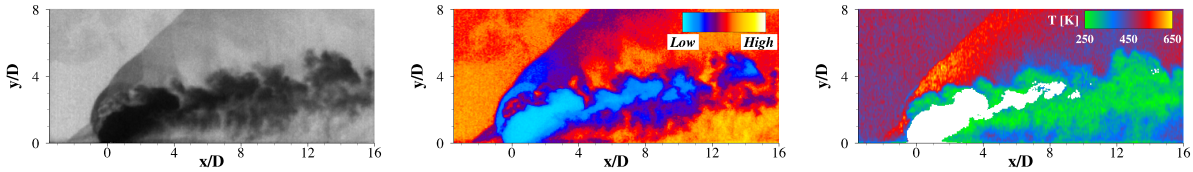


(a) (b) (c)

Figure 4: Sample of toluene PLIF images: (a) view from first camera (WG 305), (b) view from second camera (BP 280), (c) reconstructed temperature field from the ratio of the two views.

$s$ = 1.7 – 31, with corresponding values of $r$ = 1.2 – 0.3 and $Re_D \approx 3 \times 10^5 - 6.5 \times 10^5$. The cases considered in the study are summarized in Fig. 2 where a $J$= 2.4 constant curve is shown in the ($s$, $r$) plane.

The crossflow was generated by the expansion tube, which provides short-duration, moderate- to high-enthalpy supersonic flow. A moderate-enthalpy supersonic flow using nitrogen seeded with toluene vapor (0.5% by volume) as test gas was produced. To ensure uniform and repeatable seeding, the toluene/nitrogen mixture was prepared manometrically in a separate tank and then used as the test gas in the expansion tube. Throughout the study, the freestream conditions were maintained constant from shot to shot at $M_{cf} = 2.3$ ($\pm 0.1$), $p_{cf} = 1.1$ $atm$ ($\pm 0.1$ $atm$) and $T_{cf} \approx 460$ $K$ ($\pm 10$ $K$), with a test time duration of approximately 2 $ms$ (over which $M_{cf}$ was steady within 10%). The crossflow conditions reported here were estimated from a set of calibration runs and from a measure of the shock speeds from which nominal, bulk-average conditions were inferred using a zero-dimensional expansion tube solver (based on the expansion tube analysis of Trimpi (1962)). This flow condition in our expansion tube was specifically developed and characterized in Miller *et al.* (2013) for toluene PLIF imaging applications. Further details on the crossflow calibration methodology can be found in that reference. The data presented here were collected from several single-shot repetitions of the experiment repeated under nominally identical (crossflow) conditions.

## Toluene PLIF diagnostics

Planar laser-induced fluorescence (PLIF) imaging of a tracer seeded in the crossflow was used as a non-intrusive quantitative imaging technique to measure the mixing properties of the transverse jet. Temperature was used as a passive scalar tracing the mixing between the cold fluid of the traverse jet and the hot crossflow. Single-wavelength excitation, dual-band detection toluene PLIF thermometry was used. This technique results from our recent extension of single-band detection toluene PLIF imaging in supersonic flow to dual-band detection schemes for thermometry in complex supersonic flows. The method used here follows the development and optimization performed by Miller *et al.* (2013), which was here extended for mixing studies applications. Here only a brief description of the experimental system and technique is provided. Further details on toluene PLIF thermometry can be found in the cited reference.

The excitation laser light was provided by a frequency quadrupled injection seeded Nd:YAG laser. The resulting laser beam was directed to the test section where it was formed into a collimated 4 $cm$ wide laser sheet through a combination of cylindrical lenses and then focused to a (FWHM) thickness of about 0.4 mm.

Following 266 nm excitation, fluorescence was collected with two separate ICCD cameras equipped with suitable collection optics and filters. In particular, an Andor iStar 712 ($512 \times 512$ pixel) and a LaVision DynaMight ($2 \times 2$ binned to $512 \times 512$ pixel) ICCD cameras were used. The ICCD cameras were gated to 400 $ns$ to capture all fluorescence while reducing collection of unwanted background light. Each camera was viewing the imaging region from opposite sides of the laser sheet (see Fig. 3), and adjusted to match magnification and field-of-view. Initial camera registration was carried out by imaging of a suitable target and using standard image dewarping techniques, and it was later refined on a shot-to-shot basis by the help of registration marks at the edges of the laser sheet introduced by modulating the intensity of the illumination sheet at its edges.

In this dual-wavelength collection scheme, each camera collected a different spectral band of toluene fluorescence by imaging through different optical filters (see Fig. 3). In particular, the DynaMight ICCD camera was equipped with two interference bandpass filters centered at 280 $nm$ with $\pm 10$ $nm$ FWHM bandwidth (BP280) and one UG11 Schott glass filter; conversely, the iStar ICCD camera used a 3 $mm$ thick WG 305 long pass filter and UG11 filters. BP280 and WG305 filters were used to both limit the collection spectral bandwidth and to suppress excitation laser light reflections. The ratio of the two camera views, which depends only on the local fluid temperature, was then converted to temperature following the calibration procedure described in Miller *et al.* (2013).

The process of reconstructing the temperature field from each individual image is shown in Fig. 4. This figure shows (background subtracted, laser sheet nonuniform intensity corrected and dewarped) toluene PLIF images of the transverse jet as obtained by each view (Figs. 4a and 4b) and after they have been converted to temperature (Fig. 4c). Note that the pointwise PLIF signal presented in Figs. 4a and 4b is sensitive to local tracer concentration (mixing) and temperature, which results in a non-linear and non-unique correspondence between the PLIF signal and local fluid state (pressure, temperature, mixture fraction). This effect can be seen by the PLIF signal drop across the bow shock where the PLIF signal drops due to the increase of temperature even though the local fluid density increases. Toluene PLIF in fact shows an exponential sensitivity with respect to temperature (Koban *et al.*, 2005). Another example is the rendering of the mixing occurring in the windward shear layer of the transverse jet between cold pure jet fluid and hot (toluene seeded) pure crossflow fluid. The non-linear and non-unique dependance renders the mixing layer as a corresponding reaction layer that would be ob-

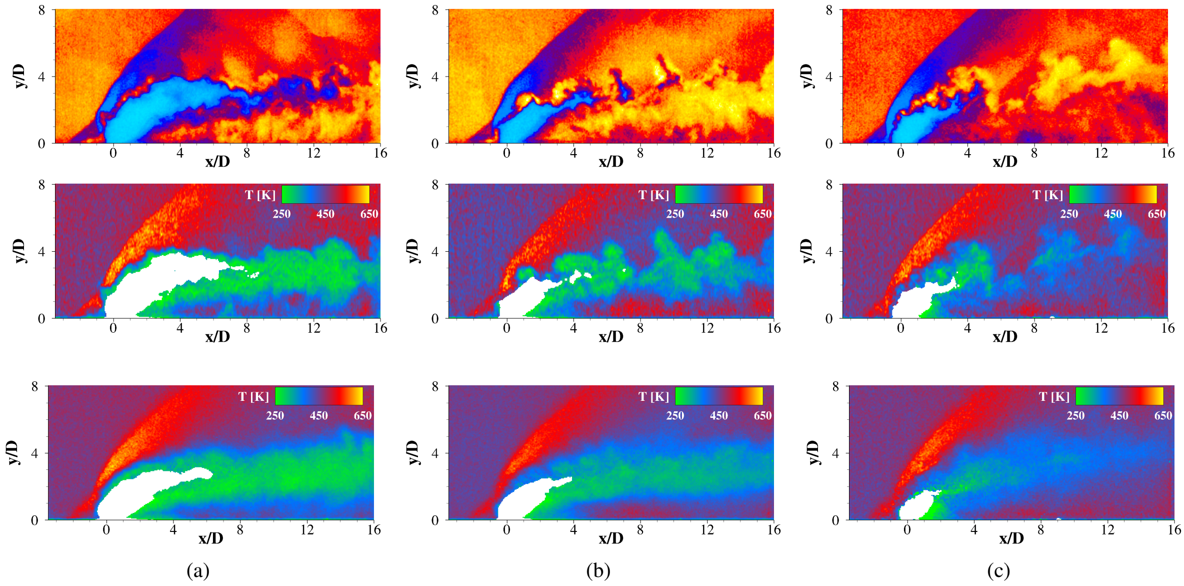

Figure 5: Instantaneous and ensemble-average turbulent structure of the transverse jet for injection of (a) $H_2$, (b) He/Ar mixture, and (c) Ar. Top: instantaneous, single-camera view (BP280) before conversion to temperature (see colormap in Fig. 4b); middle: instantaneous temperature; bottom: ensemble-average temperature.

served in a corresponding reacting flowfield (Gamba *et al.*, 2011), but in a way that is reminiscent of a cold-chemistry type of effect (Paul & Clemens, 1993).

The results of this introductory image shows that the strong temperature sensitivity of toluene PLIF is capable of capturing and effectively rendering all the major flow structures (refer back to Fig. 1): the bow shock, the separation shock, and the edge of the transverse jet. Note also that jet fluid entrainment in the upstream separation region is also well captured (Gamba *et al.*, 2011). The ratio between each view (Figs. 4a and 4b) then becomes independent of the local fluid concentration and pressure, and it retains only the temperature dependence. By applying the calibration, the ratio of signal is then converted to temperature shown in Fig. 4c. The imaging results of the raw PLIF images and of the reconstructed temperature distribution are then used for the analysis presented below.

Because the diagnostic is based on a ratiometric method involving (relatively) low signal to noise ratio (SNR) PLIF images, the resulting temperature field is of even lower SNR. In particular, for the range of temperature considered in this study, the estimated (spatial) SNR of each PLIF image is in the range 30–40, which then results in a local SNR of the reconstructed temperature of about 20–25. In other words, the local, instantaneous estimated (precision) uncertainty is about 5%.

For the purpose of this study, mixing between jet and crossflow fluids is extracted from a local measure of the fluid temperature resulting from entrainment and mixing of cold jet and hot crossflow fluids. Note, however, that owing to compressibility and presence of shock waves, the local temperature field is also controlled by shock wave systems. Finally, because toluene is injected only in the crossflow, the pure jet portion (core) of the transverse jet is not captured (see dark region in Fig. 4 and following figures where the barrel shock should be located). In order to remove false measurements in this regions, they were masked out by a local threshold based on a minimum detectable PLIF signal. On the other hand, seeding the crossflow allows one to extract the local fluid temperature also in regions away from where the transverse jet develops and thus provides a complete view of the flowfield generated by transverse injection in the supersonic crossflow.

## RESULTS

Figure 5 shows representative instantaneous PLIF (top) and temperature (middle) distributions, and the ensemble-average temperature distribution (bottom) of the JISCF for the following three cases: injection of (a) $H_2$, (b) He/Ar mixture, and (c) Ar at the same value of $J = 2.4$ (see Fig. 2). The other cases studied here show intermediate flow structures and behaviors. Analysis of multiple (single-shot) repetitions under identical conditions show similar characteristics. The ensemble-average results were computed from an ensemble of 10 single-shot experiments.

### Instantaneous results

The instantaneous results showing the structure of the JISCF for the three cases show substantial difference between different injection fluid types even though $J$ is held constant. A qualitative assessment suggests that the location of the near-field, windward shear layer is mostly unaffected by the jet fluid type, so is the location and shape (hence local strength) of the bow shock. The upstream separation also does not appear to be affected by it. The formation of this portion of the flowfield might therefore be independent of viscous and mixing effects (i.e., it is an inviscid response of the system). However, the local structure of the shear layer where mixing occurs, hence the mechanism responsible for its formation, is significantly different. In turn, this also affect the far-field structure of the shear layer.

As indicated in the previous section, the region where (molecular level) mixing occurs is well rendered by the properties of the toluene PLIF signal (cf. PLIF images). In the PLIF images of Fig. 5, the mixing portion of the shear layer is rendered as the high PLIF signal portion between the core of the jet and the post-shock region (both low PLIF signal regions). For the hydrogen case, Fig. 5a, the mixing region is a thin and regular region, which then gradually and continuously evolves into the shear layer structure of the jet far-field. The He/Ar mixture, Fig. 5b, evolves into large-scale vortical structures, which then propagate downstream in the far-field and become elongated in the direction perpendicular to the local direction of the wake flow. As a result, note the interesting finger-like structures that are clearly visible in Fig. 5b (PLIF image). For the argon case, Fig. 5c, the near-field shear layer quickly grows from small-scale structures that are readily originated at the injector exit into the large turbulent scales of the intermediate- and far-field.

The topology of these turbulent structures that define the shear layer have a strong impact of the resulting temperature distribution (mixing) of the jet fluid, cf. the instantaneous temperature images (middle row). For the hydrogen case, the wake of the jet remains at low temperature (near the stagnation temperature of the jet) and well confined. This is a result of the low entrainment, and hence mixing, that control this case. The He/Ar mixture case, the wake is controlled by the large-scale structures identified previously and results in a corrugated outer edge. Finally, for the Ar case, past the near-field, discrete large-scale structures with what seems a periodic spacing remain well defined and control the dynamics of the wake. These features, then, result in generally higher values of the wake temperature, suggesting faster mixing.

The observe change in the structure of the mixing layer at the windward near-field side can be attributed to an effect due to $r$. The characteristics of compressible mixing layers are found to depend on a combination of ($s$, $r$) and by a compressibility parameter, which has been found to be a convective Mach number $M_c$ based on a suitable convection velocity $U_c$ (Papamoschou & Roshko, 1988, see cited references for their derivation and definition). In these experiments, going from $H_2$ to Ar, $r$ is decreased to about 0.3, with a corresponding increase in $M_c$ from about 0.1 to near 1. In two-dimensional (2D) compressible mixing layer, larger velocity differences (i.e., $r$) drive the mixing layer itself; however, large values of $M_c$ are found to decrease the growth of mixing layer width, hence mixing. This traditional result found in 2D compressible mixing layers does not seem to apply to the near-field shear layer of the JISCF system. In fact, as $r$ diverges from unity and as the corresponding value of $M_c$ increases, the results of Fig. 5 show that the shear layer width and the resulting mixing substantially increases.

A qualitative evaluation of the trajectory of the outer edge of the wake or of the large-scale turbulent structures that are detected, indicate that the trajectory of these structures appear to have some dependance on jet fluid type, ($r$, $s$). In fact, the Ar cases appears to generated large-scale structures that penetrate a bit further even though they encounter faster mixing. To further investigate this, the discussion of the ensemble-average results below is presented.

## Ensemble-average results

The last row of images in Fig. 5 show the ensemble-average temperature distribution of the three selected cases. Note that only 10 shots were used in the averaging, and the mean results are certainly not statistically converged. Nevertheless the main characteristics of the JISCF system are well rendered. The lack of mixing in the $H_2$ case relative to

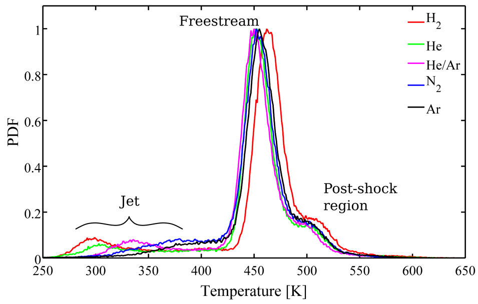


Figure 6: PDF of the ensemble-average temperature for different injection fluids. The PDF is computed from all valid data point measurements in the plane.

the Ar case is readily apparent. In the former case, a long, jet-fluid rich core persists far downstream where the shear layer remains well organized; in the latter case, the core of the jet quickly breaks down (the core quickly closes in itself just downstream of the injector). Note that the masked out region refer to the core of the jet where jet-fluid rich flow exists. The Ar case shows a length of this core region substantially smaller than the $H_2$ even though the injection pressure is nearly the same (it varies by less than 10%). This is another indication of the faster molecular level mixing that is observed in the Ar case relative to $H_2$ case (or other intermediate cases).

To further quantify the level of mixing provided by the different injection cases, probability density functions (PDF) of the local ensemble-average temperature were computed from the ensemble-average results of Fig. 5. The results are shown in Fig. 6 and are computed from all valid points (i.e., other than points in the core of the transverse jets where measurements could not be extracted from). For all cases, we can recognize two regions: the region of high average temperature, which corresponds to crossflow regions, and the region of low average temperature, which corresponds to the region of the jet wake. The portion of the PDF curve that refers to the crossflow is nearly the same for all cases (other than the $H_2$ case that shows a shifted profile) since the freestream was kept constant (and neglecting small systematic variations due to the operation of the facility, which for example explains the shift for the $H_2$ case). Furthermore, the range of most probable values corresponds to a measure of the freestream temperature, which, from these measurements, is found to be about 460 $K$ $\pm 10$ $K$. This value compares well with what inferred from shock speed measurements.

The portion of the curve at low temperature refers to the region of the jet wake. For the $H_2$ case, the is a second peak near 290 $K$ (which is the injection temperature of the jet). For heavier jet fluids, this peaks moves at larger temperature, until it is smeared out and disappears for the heavy jet cases ($N_2$ and Ar). Figure 6 further quantifies the level of mixing (in an average sense) and its dependance on the injectant type.

Finally, to assess the impact of injectant on the average transverse jet penetration, the average temperature distribution along the $y-$direction (wall-normal) is plotted in Fig. 7. The general conclusion that the Ar case resulted in more effective mixing is also supported by this result. Furthermore, we can also observe that based on the definition of penetration, we might reach a different conclusion on what

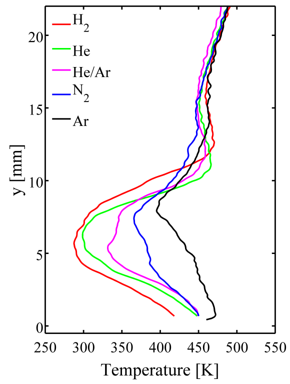


Figure 7: Average temperature profile in the wake of the JISCF. The profile was extracted from $x-$direction averaging the band $12.5 \leq x/D \leq 15$.

is the effective penetration of each case. For example, the point of minimum average temperature is seen to move outward as heavier jet fluids are used (from $y/D \approx 5$ with $H_2$ to $y/D \approx 8$ with Ar). However, the $y-$location of the outer point of the temperature profile in the wake has less dependency on the jet properties. This indicates that the overall penetration of the JISCF is weakly affected by the details of injection but it is primary controlled by $J$.

## CONCLUSIONS

The results of this work indicate that, in spite of similar value of $J$ and similar average jet penetration, the mixing properties and the structure of the transverse jet (both instantaneous and average), have a strong dependance on injection details. The instantaneous turbulent structure of the jet is significantly different under different $(r, s)$ conditions. Since these structures and their dynamics control the local entrainment and mixing processes, then mixing itself is directly affected by low (high) values of the $s$ $(r)$ compared to the corresponding case at high (low) values.

The assessment of Portz & Segal (2006) on JISCF penetration suggests that the average jet penetration have a very weak sensitivity to the molecular weight of the injected species and it can effectively be ignored. Their result is supported by our findings. Therefore, although there is a weak dependence (and perhaps arbitrariness) on the exact definition of jet penetration, this global quantity might be insensitive to injectant properties while the resulting underlying mixing appears to have a strong dependance on it.

**Acknowledgements** This work was performed with the auspices of the Department of Energy sponsored Predictive Science Academic Alliance Program (PSAAP) at Stanford University.

## REFERENCES

Ben-Yakar, A., Mungal, M. G. & Hanson, R. K. 2006 Time evolution and mixing characteristics of hydrogen and ethylene transverse jets in supersonic crossflows. *Physics of Fluids* **18**.

Broadwell, J. E. & Breidenthal, R. E. 1984 Structure and mixing of a transverse jet in incompressible flow. *J. Fluid Mech.* **148**, 405–412.

Fric, T. F. & Roshko, A. 1994 Vortical structure in the wake of a transverse jet. *J. Fluid Mech.* **279**, 1–47.

Gamba, M., Mungal, M. G. & Hanson, R. K. 2011 Ignition and near-wall burning in transverse hydrogen jets in supersonic crossflow. *49th AIAA Aerospace Sciences Meeting and Aerospace Exposition, Jan. 4-7, Orlando, Florida. Paper No. AIAA-2011-0319. AIAA Propellants and Combustion Best Paper Award* .

Getsinger, D. R., Hendrickson, C. & Karagozian, A. R. 2012 Shear layer instabilities in low-density transverse jets. *Exp. Fluids* **53**, 783–801.

Gruber, M. R., Nejad, A. S., Chen, T. H. & Dutton, J. C. 1996 Bow shock/jet interaction in compressible transverse injection flowfields. *AIAA J.* **34** (10), 2191–2193.

Gruber, M. R., Nejad, A. S., Chen, T. H. & Dutton, J. C. 1997 Compressibility effects in supersonic transverse injection flowfields. *Physics of Fluids* **9** (5), 1448–1461.

Hasselbrink, E. F. & Mungal, M. G. 2001 Transverse jets and jet flames. part 1. scaling laws for strong transverse jets. *J. Fluid Mech.* **443**, 1–25.

Heltsley, W. N., Snyder, J. A., Houle, A. J., Davidson, D.F., Mungal, M. G. & Hanson, R. K. 2006 Design and characterization of the stanford 6 inch expansion tube. In *42nd AIAA/ASME/SAE/ASEE Joint Propulsion Conference & Exhibit, 9 - 12 July, AIAA Paper No. AIAA-2006-4443*.

Karagozian, A. R. 2010 Transverse jets and their control. *Progress in Energy and Combustion Science* **36** (5), 531–553.

Koban, W., Koch, J. D., Hanson, R. K. & Schulz, C. 2005 Toluene LIF at elevated temperatures: implications for fuel-air ratio measurements. *App. Phys. B: Lasers and Optics* **80**, 147–150.

Mahesh, K. 2013 The interaction of jets with crossflow. *Annu. Rev. Fluid. Mech.* **45**, 379–407.

Megerian, S., Davitian, J., De B. Alves, L. S. & Karagozian, A. R. 2007 Transverse-jet shear layer instabilities. part 1. experimental studies. *J. Fluid Mech.* **593**, 93–129.

Miller, V. A., Gamba, M., Mungal, M. G. & Hanson, R. K. 2013 Single- and dual-band collection toluene PLIF thermometry in supersonic flows. *Submitted to Exp. Fluids* .

Papamoschou, D. & Roshko, A. 1988 The compressible turbulent shear layer: an experimental study. *J. Fluid Mech.* **197**, 453–477.

Paul, P. H. & Clemens, N. T. 1993 Subresoltuion measurements of unmixed fluid using electronic quenching of NO $A^2\Sigma^+$. *O. Letters* **18** (2), 161–163.

Portz, R. & Segal, C. 2006 Penetration of gaseous jets in supersonic flows. *AIAA J.* **44** (10), 2426–2429.

Schetz, J. A. & Billig, F. S. 1966 Penetration of gaseous jets injected into a supersonic stream. *J. Spacecraft* **3** (11), 1658–1665.

Smith, S. H. & Mungal, M. G. 1998 Mixing, structure and scaling of the jet in crossflow. *J. Fluid Mech.* **357**, 83–122.

Su, L. & Mungal, M. G. 2004 Simultaneous measurements of scalar and velocity field evolution in turbulent crossflowing jets. *J. Fluid Mech.* **513**, 1–45.

Trimpi, R. L. 1962 A preliminary theoretical study of the expansion tube, a new device for producing high-enthalpy short-duration hypersonic gas flows. *Tech. Rep.*. NASA TR R-133.

Watanabe, J., Kouchi, T., Takita, K. & Masuya, G. 2012 Large-eddy simulation of jet in supersonic crossflow with different injectant species. *AIAA J.* **50** (12), 2765–2778.